Position Control for Interior Permanent Magnet Synchronous Motors using an Adaptive Integral Binary Observer

Hyoung-Seok kang†, Cheon-Kyu Kim* and Young-Seok Kim**

Abstract – An approach to control the position for an interior permanent magnet synchronous motor (IPMSM) based on an adaptive integral binary observer is described. The binary controller with a binary observer is composed of a main loop regulator and an auxiliary loop regulator. One of its key features is that it alleviates chatter in the constant boundary layer. However, steady state estimation accuracy and robustness are dependent upon the thickness of the constant boundary layer. In order to improve the steady state performance of the binary observer and eliminate the chattering problem of the constant boundary layer, a new binary observer is formed by adding extra integral dynamics to the existing switching hyperplane equation. Also, the proposed adaptive integral binary observer applies an adaptive scheme because the parameters of the dynamic equations such as the machine inertia and the viscosity friction coefficient are not well known. Furthermore, these values can typically be easily changed during normal operation. However, the proposed observer can overcome the problems caused by using the dynamic equations, and the rotor position estimation is constructed by integrating the rotor speed estimated with a Lyapunov function. Experimental results obtained using the proposed algorithm are presented to demonstrate the effectiveness of the approach.

Keywords: IPMSM, Sensorless, Binary, Observer, Position control

1. Introduction

Recent developments in power semiconductor technology, digital electronics, magnetic materials and control algorithms have enabled modern AC motor drives to meet challenging high efficiency and high performance requirements in the industrial sector. In high performance applications, the interior permanent magnet synchronous motor (IPMSM) has seen growing popularity as compared to other types of AC motors due to advantageous features such as a high torque to inertia ratio, superior power density, high efficiency, low noise, and robust operation [1][2]. In order to position control and achieve high performance of the IPMSM, it is necessary to know the absolute position of the rotor. To this end, an absolute encoder or resolver has been used for sensing the rotor position. These position sensors, however, require a special arrangement for mounting and decrease the reliability of the system. Hence, there has been increased interest in developing position sensorless control algorithms [3].

Research on changing observers for speed sensors has been conducted. The sliding mode control (SMC) algorithm has been widely studied in the field of motion control. The drawback of the SMC, however, is that the resulting control input is discontinuous on the sliding surface. Consequently, switching of the control input theoretically occurs at infinite frequency. However, the frequency is not infinitely high due to the finite switching time in real applications. Therefore, the SMC features an inevitable chattering phenomenon which is undesirable for electrical rotor mechanisms. Furthermore, unexpected instability arises due to delay and hysteresis [4][5].

To overcome these problems of the SMC, binary control has been adopted and applied to the position sensorless vector control of the IPMSM. Binary control can be thought of as a generalization of the SMC. A key difference between the two forms of control is that binary control does not explicitly use a reference model. A binary observer using binary control consists of a main loop regulator and an auxiliary loop regulator, as does the binary controller. Hence, the binary observer can alleviate chattering while retaining the benefits achieved with a sliding mode observer. However, the auxiliary loop regulator continuously changes the gain of the main loop regulator in the domain referred to as the constant boundary layer, and estimation errors also occur [6]-[7] Thus, in order to improve the steady state performance of the binary observer, the binary observer is formed by adding extra integral augmented switching to the hyperplane equation. By means of integral characteristics, the rotor speed can be finely estimated and utilized as a sensorless speed controller for an IPMSM. Because the parameters of the dynamic equations such as the machine inertia and the viscosity friction coefficient are not well known, and these values can be easily changed during normal operation, there are many restrictions in an actual implementation. Owing to these problems, a sensorless algorithm that eliminates the mechanical equation of the IPMSM is implemented using an adaptive scheme. The proposed adaptive integral binary observer applies an adaptive scheme so that the observer can over-

† Corresponding Author : Samsung Techwin Co., LTD. (hyounseok.kang@samsung.com)
* LG Electronics Co., LTD. (ck_kim@lge.co.kr)
** Dept. of Electrical and Electronic Engineering, Inha University, Korea (youngsk@inha.ac.kr)
Received 7 January 2009; Accepted 7 May 2009

come the problems caused by using dynamic equations. A Lyapunov function is used to prove that the system stability included speed estimation and speed control [8].

In this paper, the design method of the proposed binary observer with an integral augmented switching hyperplane and speed estimator using an adaptive scheme for sensorless vector control of the IPMSM is presented. From experimental results, the proposed observer is found to have good estimation performance without chattering problems or estimation errors.

2. Integral Binary Observer

2.1 Integral Binary Observer

In the stationary reference frame $(\alpha-\beta)$, the voltage equation of the IPMSM is as follows:

$$\frac{di_s}{dt} = Ai_s + L_1 v_s + L_1 E_s + Bi_s \tag{1}$$

where $i_s = [i_\alpha \quad i_\beta]^T$: stator α - and β - axes currents

$v_s = [v_\alpha \quad v_\beta]^T$: stator α - and β - axes voltages

$E_s = [E_\alpha \quad E_\beta]^T$: induced voltages

$E_\alpha = -K_E \omega \sin\theta$, $E_\beta = K_E \omega \cos\theta$

$A = -RL_1$, $B = -\omega(L_d - L_q)L_2$

R : stator resistance

L_d : d - axes inductance

L_q : q - axes inductance

K_E : back EMF constant

ω : rotor speed

θ : rotor position

$$L_1 = \begin{bmatrix} \frac{1}{L_d} & 0 \\ 0 & \frac{1}{L_q} \end{bmatrix}, \quad L_2 = \begin{bmatrix} 0 & \frac{1}{L_d} \\ \frac{1}{L_q} & 0 \end{bmatrix}$$

The adaptive integral binary observer is composed of the voltage equations of the IPMSM without the motion equation in state equation.

From (1), the binary observer is constructed with the following structure:

$$\frac{d\hat{i}_s}{dt} = A\hat{i}_s + L_1 v_s + L_1 \hat{E}_s + B\hat{i}_s - K\gamma_s \tag{2}$$

where $\hat{}$: Estimated value

$\mathbf{K} = \begin{bmatrix} k_\alpha & 0 \\ 0 & k_\beta \end{bmatrix}$: Constant

$\gamma_s = [\gamma_\alpha \quad \gamma_\beta]^T$: Input of the binary observer

Integral switching hyperplanes are defined by:

$$\sigma = (\sigma_\alpha, \sigma_\beta) = 0 \tag{3}$$

where $\sigma_\alpha = -ce_\alpha - \int_0^t e_\alpha d\tau, e_\alpha = \hat{i}_\alpha - i_\alpha$

$\sigma_\beta = -ce_\beta - \int_0^t e_\beta d\tau, e_\beta = \hat{i}_\beta - i_\beta$

c : Positive constant

Also, the boundary layer is represented by:

$$G_\delta = \sigma^+(t)\sigma^-(t) \le 0 \tag{4}$$

$$\sigma^+(t) = \sigma(t) - c\delta, \quad \sigma^-(t) = \sigma(t) + c\delta$$

where δ : Constant, $0 \le \delta < 1$

Error dynamics are obtained by subtracting (1) from (2), respectively.

$$\dot{e}_s = \frac{d}{dt}(\hat{i}_s - i_s) = A(\hat{i}_s - i_s) + (B\hat{i}_s - Bi_s) + L_1(\hat{E}_s - E_s) - K\gamma_s \tag{5}$$

where $\mathbf{e}_S = [e_\alpha \quad e_\beta]^T = [\hat{i}_\alpha - i_\alpha \quad \hat{i}_\beta - i_\beta]^T$

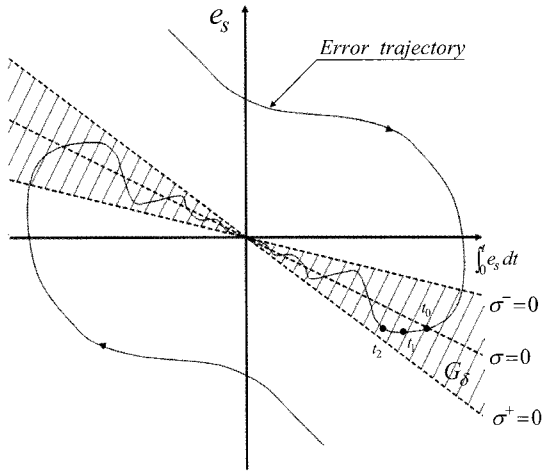

Fig. 1. Phase plane trajectory of the binary observer

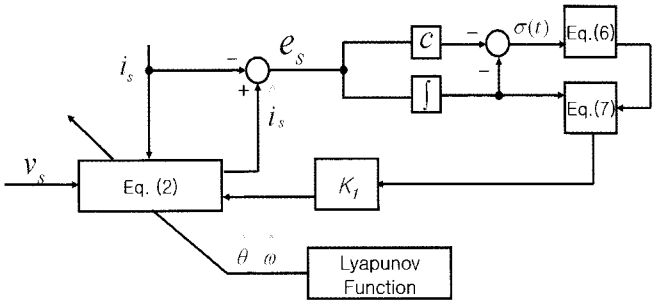

Fig. 2. Block diagram of an adaptive integral binary observer

As compared with the sliding mode observer, the chattering problem of the binary observer is alleviated. However, the accuracy of the estimation depends strongly upon the thickness of the boundary layer, as shown in Fig. 1. To reduce the error of the steady state, as can be seen in (3), a binary observer with integral switching hyperplanes is used. The integral switching hyperplane of the binary observer is defined by the error of the estimation current and the real current. The structure of the binary observer is shown in

Fig. 2. From Fig. 1, the trajectory of the error departs from an initial estimation error e_s, reaches the boundary layer, and converges along the horizontal axis until $e_s = 0$.

Continuous switching inputs are defined as follows.
The main loop regulator:

$$\begin{bmatrix} \gamma_\alpha \\ \gamma_\beta \end{bmatrix} = \begin{bmatrix} \mu_\alpha \mid e_\alpha \mid \\ \mu_\beta \mid e_\beta \mid \end{bmatrix} \tag{6}$$

The auxiliary loop regulator:

$$\begin{bmatrix} \dot{\mu}_\alpha \\ \dot{\mu}_\beta \end{bmatrix} = -\alpha \begin{bmatrix} \mu_\alpha + sat(\lambda_\alpha) \\ \mu_\beta + sat(\lambda_\beta) \end{bmatrix} \tag{7}$$

Where $\lambda_\alpha = \sigma_\alpha / c\delta$, $\lambda_\beta = \sigma_\beta / c\delta$

The block diagram in Fig. 2 represents the proposed binary observer for position sensorless drives. If all errors of the binary observer exist in the boundary layer G_δ, errors never escape the domain G_δ; this is called a G_δ invariant condition. Therefore, (8) must be satisfied on the boundary of the domain G_δ. Also, if the main loop regulator gain K and the auxiliary loop regulator gain α are established in order to satisfy (8), the binary observer will be superior to the conventional binary observer and robust to chattering.

$$\sigma^+(t) \cdot \dot{\sigma}^+(t) < 0, \quad \sigma^-(t) \cdot \dot{\sigma}^-(t) < 0 \tag{8}$$

2.2 Derivation of the gain K

The main loop regulator gain k_α can be obtained from the invariant condition G_δ. In the condition where $\alpha(t)$ exists in the boundary layer G_δ, above all, if $\sigma_\alpha > 0$, from the inequality (9), the gain k_α must be satisfied (10).

$$\sigma_\alpha \cdot \dot{\sigma}_\alpha = \sigma_\alpha \left\{ -c_\alpha \left[-\frac{R}{L_d} e_\alpha - \left(\frac{L_d - L_q}{L_d}\right)(\hat{\omega} i_\beta - \omega i_\beta) + \frac{K_E}{L_d}(\hat{\omega}\sin\hat{\theta} - \omega\sin\theta) + k_\alpha \gamma_\alpha \right] - e_\alpha \right\} < 0 \tag{9}$$

$$k_\alpha > \frac{1}{(1-h)\delta}\left[\left(-\frac{R}{L_d} + \frac{1}{c_\alpha}\right)\delta + \left(\frac{L_d - L_q}{L_d}\right)(\hat{\omega} i_\beta - \omega i_\beta) + \frac{K_E}{L_d}(\hat{\omega}\sin\hat{\theta} - \omega\sin\theta) \right] \tag{10}$$

where $0 < h < 1$

Also, if $\sigma(t) < 0$, the result given by (11) can be deduced.

$$k_\alpha > -\frac{1}{(1-h)\delta}\left[\left(-\frac{R}{L_d} + \frac{1}{c_\alpha}\right)\delta + \left(\frac{L_d - L_q}{L_d}\right)(\hat{\omega} i_\beta - \omega i_\beta) + \frac{K_E}{L_d}(\hat{\omega}\sin\hat{\theta} - \omega\sin\theta) \right] \tag{11}$$

From (10) and (11), k_α is derived to satisfy (12).

$$k_\alpha > \frac{1}{(1-h)\delta}\sup_{t \geq t_0}\left| \left(-\frac{R}{L_d} + \frac{1}{c_\alpha}\right)\delta - \left(\frac{L_d - L_q}{L_d}\right)(\hat{\omega} i_\beta - \omega i_\beta) + \frac{K_E}{L_d}(\hat{\omega}\sin\hat{\theta} - \omega\sin\theta) \right| \tag{12}$$

In the same manner, k_β is derived as follows:

$$k_\beta > \frac{1}{(1-h)\delta}\sup_{t \geq t_0}\left| \left(-\frac{R}{L_q} + \frac{1}{c_\beta}\right)\delta + \left(\frac{L_d - L_q}{L_q}\right)(\hat{\omega} i_\alpha - \omega i_\alpha) + \frac{K_E}{L_q}(\hat{\omega}\cos\hat{\theta} - \omega\cos\theta) \right| \tag{13}$$

Therefore, from (12) and (13), the domain of K can be derived as follows:

$$K > \frac{1}{(1-h)\delta}\max\left[\begin{array}{l} \sup_{t \geq t_0}\left| \left(-\frac{R}{L_d} + \frac{1}{c_\alpha}\right)\delta + \left(\frac{L_d - L_q}{L_d}\right)(\hat{\omega} i_\beta - \omega i_\beta) + \frac{K_E}{L_d}(\hat{\omega}\sin\hat{\theta} - \omega\sin\theta) \right|, \\ \sup_{t \geq t_0}\left| \left(-\frac{R}{L_q} + \frac{1}{c_\beta}\right)\delta + \left(\frac{L_d - L_q}{L_q}\right)(\hat{\omega} i_\alpha - \omega i_\alpha) + \frac{K_E}{L_q}(\hat{\omega}\cos\hat{\theta} - \omega\cos\theta) \right| \end{array} \right] \tag{14}$$

2.3 Derivation of the gain α

When $\lambda(t) = \sigma(t) / c\delta$, where the state of the system passes through $\sigma = 0$, t_1 is defined, and t_2 is defined as time to reach the boundary of the domain in $\sigma > 0$. (7) is then derived as follows:

$$t_2 - t_1 < \frac{1}{\alpha}\ln\frac{4}{2h-1} \tag{15}$$

where $t_2 > t_1$, t_1 is time when $\lambda(t) = 1/2$,
t_2 is time when, $\lambda(t) = 1$
$0.5 < h < 1$

In the case of $\sigma > 0$, α is derived to be $\mu(t) \leq -(1-h)$. Also, supposing $\mu(t_2) > -(1-h)$ by using the contradiction method, we can obtain the function $\lambda(t_2)$ in $[t_1, t_2]$ for $\lambda(t_2) \geq 1/2$.

$$\lambda(t_2) \leq \frac{1}{2} + \frac{1}{c\delta}\overline{K}_0(t_2 - t_1) \tag{16}$$

Where

$$\overline{K}_0 = \max\left[\begin{array}{l} \sup_{t \geq t_0}\left| -c_\alpha\left[\left(-\frac{R}{L_d}\right)\delta + \left(\frac{L_d - L_q}{L_d}\right)(\hat{\omega} i_\beta - \omega i_\beta) + \frac{K_E}{L_d}(\hat{\omega}\sin\hat{\theta} - \omega\sin\theta) + \frac{K_E}{L_d}(\hat{\omega}\sin\hat{\theta} - \omega\sin\theta) + k_1\gamma_\alpha \right] - e_\alpha \right|, \\ \sup_{t \geq t_0}\left| -c_\beta\left[\left(-\frac{R}{L_q}\right)\delta + \left(\frac{L_d - L_q}{L_q}\right)(\hat{\omega} i_\alpha - \omega i_\alpha) + \frac{K_E}{L_d}(\hat{\omega}\cos\hat{\theta} - \omega\cos\theta) + \frac{K_E}{L_q}(\hat{\omega}\cos\hat{\theta} - \omega\cos\theta) + k_1\gamma_\beta \right] - e_\beta \right| \end{array} \right]$$

When we assume that the gain α is satisfied in inequality (15).

$$\alpha \geq \frac{2\overline{K}_0}{c\delta} \ln \frac{4}{2h-1} \tag{17}$$

(17) is rearranged using (16), substituting it into (18). The function $\lambda(t_2)$ is then given as follows:

$$\lambda(t_2) < 1 \tag{18}$$

The result of (18) contradicts the equation $\lambda(t_2) = 1$. This means that if the inequality (17) is always satisfied, the magnitude of $\mu(t)$ must have the following relation:

$$|\mu(t)| \geq 1 - h \tag{19}$$

2.4 Estimator of speed

In order to estimate rotor speed and angle, an adaptive integral binary observer is constructed using a Lyapunov function. The Lyapunov function V is chosen as:

$$\mathbf{V} = \frac{1}{2}\mathbf{e}_S^T\mathbf{e}_S + \frac{(\hat{\omega}-\omega)^2}{2} \tag{20}$$

Under the assumption that the rotor speed is constant within one sample period of the control system, derivation of the Lyapunov function is obtained as follows:

$$\dot{V} = \mathbf{e}_S^T \cdot \dot{\mathbf{e}}_S + (\hat{\omega}_r - \omega_r) \cdot \dot{\hat{\omega}} \tag{21}$$

Substituting (4) into (21), the following equation is obtained:

$$\dot{V} = \mathbf{e}_S^T[\mathbf{A}(\hat{\mathbf{i}}_s - \mathbf{i}_s) - (\hat{B}\hat{\mathbf{E}}_s - B\mathbf{E}_s) + L_1(\hat{E}_s + E_s) + K_1\gamma_s] + \Delta\omega\dot{\hat{\omega}} \tag{22}$$

Where $\Delta\omega = \hat{\omega} - \omega$

From Lyapunov's stability theory, $V > 0$ and $\dot{V} < 0$ are always satisfied when the observer is stable. Therefore, in order to satisfy $\dot{\hat{V}} < 0$, they are separated into the following, respectively:

$$e^T\left[(\hat{B}-B)\hat{i}_s + L_1(\hat{E}-E)\right] + \Delta\omega\dot{\hat{\omega}} = 0 \tag{23}$$

$$e^T\left[A(\hat{i}_s - i_s) + B(\hat{i}_s - i_s) - K\gamma_s\right] < 0 \tag{24}$$

In order to derive the rotor speed, (23) must be zero. The inequality of (24) should then be smaller than zero, and thus (20) is satisfied.

From (24), the inequality (25) can be derived as:

$$K > \frac{1}{(1-h)\delta} \max \left| \begin{array}{l} \left|(-\frac{R}{L_d} + \frac{1}{c_\alpha})\delta + \left(\frac{L_d - L_q}{L_d}\right)(\hat{\omega}\hat{i}_\beta - \omega i_\beta)\right| \\ \left|(-\frac{R}{L_q} + \frac{1}{c_\beta})\delta + \left(\frac{L_d - L_q}{L_q}\right)(\hat{\omega}\hat{i}_\alpha - \omega i_\alpha)\right| \\ + \frac{K_E}{L_d}(\hat{\omega}\sin\hat{\theta} - \omega\sin\theta) \\ + \frac{K_E}{L_q}(\hat{\omega}\cos\hat{\theta} - \omega\cos\theta) \end{array} \right| \tag{25}$$

The range of K must be set to satisfy the inequality of (14) and (25). Also, to estimate the rotor speed, (23) is rearranged as follows:

$$e^T \bullet \left[K_E \begin{bmatrix} \frac{1}{L_d} & 0 \\ 0 & \frac{1}{L_q} \end{bmatrix} \left(\hat{\omega} \begin{bmatrix} \sin\hat{\theta} \\ \cos\hat{\theta} \end{bmatrix} - \omega \begin{bmatrix} \sin\theta \\ \cos\theta \end{bmatrix} \right) \right.$$
$$\left. - (\hat{\omega} - \omega)(L_d - L_q) \begin{bmatrix} 0 & \frac{1}{L_d} \\ \frac{1}{L_q} & 0 \end{bmatrix} \hat{i}_s \right] + (\hat{\omega} - \omega)\dot{\omega} \tag{26}$$

From (26), if $\hat{\theta} \cong \theta$, estimation algorithms of the rotor speed should be derived as

$$\dot{\hat{\omega}} = -K_E\left(\frac{1}{L_d}e_\alpha \bullet \sin\hat{\theta} - \frac{1}{L_q}e_\beta \bullet \cos\hat{\theta}\right) + \left[\frac{(L_d - L_q)}{L_d}e_\alpha \hat{i}_\beta + \frac{(L_d - L_q)}{L_q}e_\beta \hat{i}_\alpha\right] \tag{27}$$

(27) includes the difference between the inductions of L_d and L_q, and gives the characteristic of the IPMSM. The estimated rotor angle $\hat{\theta}$ is obtained by integrating with the estimation speed. An overall block diagram of the sensorless algorithm using the proposed adaptive integral binary observer is shown in Fig. 3.

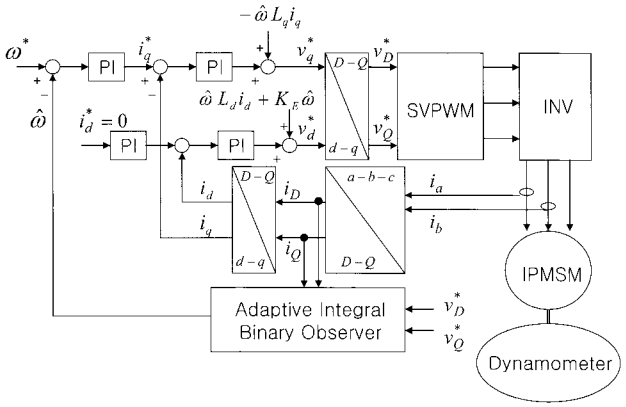

Fig. 3. Overall block diagram of the sensorless algorithm using the proposed observer

3. Experimental Results

The overall system using the adaptive integral binary observer for the IPMSM drives is shown in Fig. 4. The overall system consists of the power supply, the IPMSM, the three-phase voltage source inverter (VSI), and a Dynamometer with the control for the load. The actual parameters of the IPMSM used for experiments are listed in Table 1. The three-phase VSI is constructed using an IGBT, and a gate-firing logic to implement space-vector-modulation is developed using a motion coprocessor (ADMC201). All of the proposed algorithms are implemented using a TMS320C31

and calculations, except for the inverter voltage control, are performed by the DSP with a sampling time of 200[μs]. In order to control the current of the current controller, a-phase and b-phase are measured while c-phase is calculated. Only the information for displaying the actual speed and position is measured by an optical encoder installed at the motor shaft. Also, to align the initial position of the rotor flux at the stator α -axis, voltage pulse was injected into phase-a, and then the rotor position was zero.

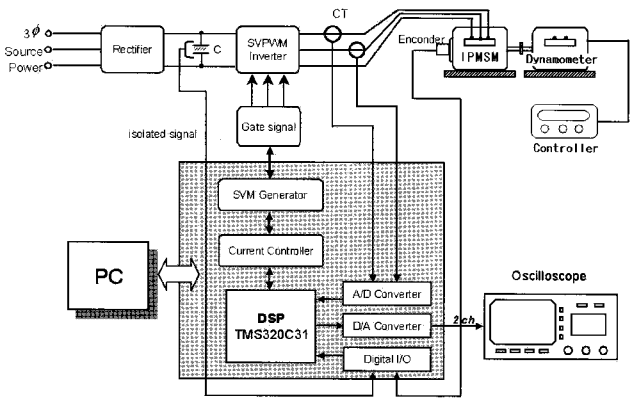

Fig. 4. Overall IPMSM drive system

Table 1. Motor parameters

Rated power	1.8	kW
Pole number	8	poles
Stator resistance	0.22	Ω
Stator inductance	0.88	mH
Torque rating	5.88	N.m
Rotor inertia	0.00186	[kg·m2]
Back emf constant	0.498	V/rad/s

Fig. 5 shows the real and estimated speed when the speed was changed from 2000rpm to –2000rpm with no load. Even when the speed was suddenly varied, the estimated speed follows the real speed closely using the proposed algorithm. Fig. 6 shows the real and estimated speed of the sensorless control with no load at 1000rpm, and Fig. 7 shows the real and estimated speed when the speed was changed from 1000rpm to – 1000rpm with no load. From Figs. 5 and 7, it is seen that the real speed at the transient as well as the steady state has good following performance for the reference within 0.2 seconds. Fig. 8 shows the real and estimated speed of the sensorless control with no load at 50rpm. Fig. 9 shows the real and estimated speed when the speed was changed from 50rpm to -50rpm. The incremental encoder measures the actual speed and has an output of 5000 pulses per revolution per minute. The counter device counts four times for each output pulse. The encoder pulses increase the average single pulse during a sample time at 50rpm. Therefore, in Figs. 8 and 9, the real speed has poor resolution. At the start of the low speed region, the estimated speed has a slight error, but quickly converges to the real speed.

Figs. 10, 11 and 12 show the real and estimated position where the speed changes rapidly, and the speed is reversed from 2000rpm to -2000rpm, 1000rpm to -1000rpm and 50rpm to -50rpm, respectively. Although the rotation direction of the IPMSM is suddenly reversed with no load, the estimated position of rating and low speed regions closely follow the real position with implementation of the proposed algorithm. Also, there is almost no error between the real and estimated position.

Fig. 13 shows the real and estimated speed for the rating speed region when the load is changed from 0% to 70% and returns to 0%. From 5.4 to 11 seconds, when a 70% step load is imposed in the steady state, the real and estimated speeds follow the reference speed after 0.8 second. Fig. 14 shows the line current and estimated speed when the speed was reversed from 2000rpm to -2000rpm with a 70% load. Although the speed is suddenly reversed with a 70% load, the estimated speed rapidly converges in the steady state without error. Fig. 15 illustrates the real and estimated speed at 1000rpm when the load is changed from 0% to 100% and returns to 0%. Fig. 16 illustrates the line current and line to line voltage when the IPMSM is driven at 1000rpm with a 100% load. In Fig. 15, estimated speed has little vibration, but the real speed follows the reference speed without error. From Figs. 13 to 16, the proposed observer can confirm robustness to the speed and load change.

Figs. 17 and 18 show the change of α loop and estimated speed when the IPMSM is driven at 1000rpm with no load, respectively. In Fig. 17, at the commencement of a transient state, the change of the α-main loop and α-auxiliary loop does not show regular alteration whereas the change is regular at the steady state.

Figs. 19 and 20 show the real and estimated position when the IPMSM is driven at 1000rpm with the error between the d-axis and electric angle. Fig. 19 illustrates the real and estimated position when the error between them is 20degrees. Fig. 20 shows the error between them at 60 degrees. After 1 rpm, the real and estimated position is united. Therefore, the robustness is confirmed despite being the starting error when the IPMSM was started.

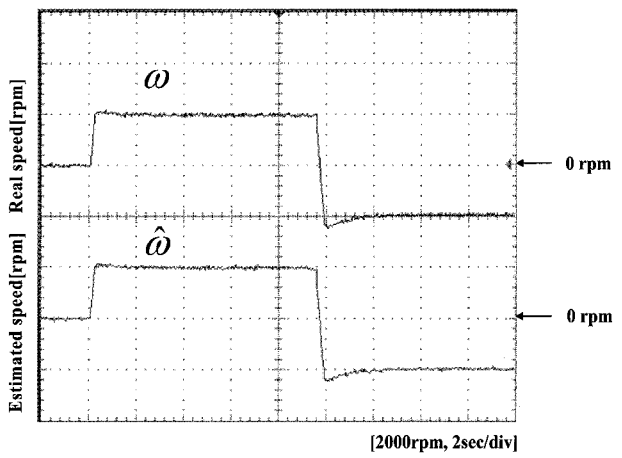

Fig. 5. Real (upper) and estimated speed (lower) when the speed is reversed from 2000rpm to -2000rpm with no load

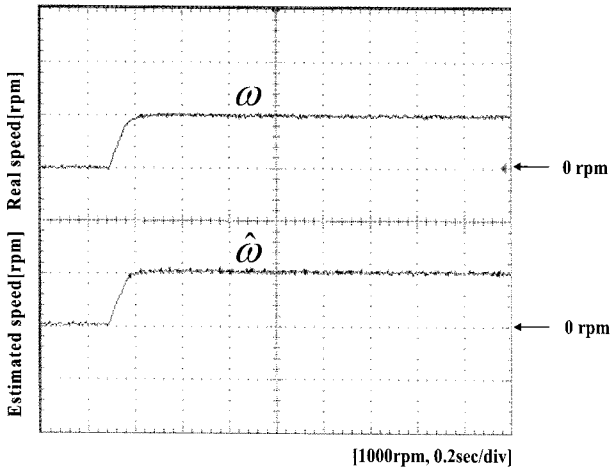

Fig. 6. Real (upper) and estimated speed (lower) when the IPMSM is driven at 1000[rpm] with no load.

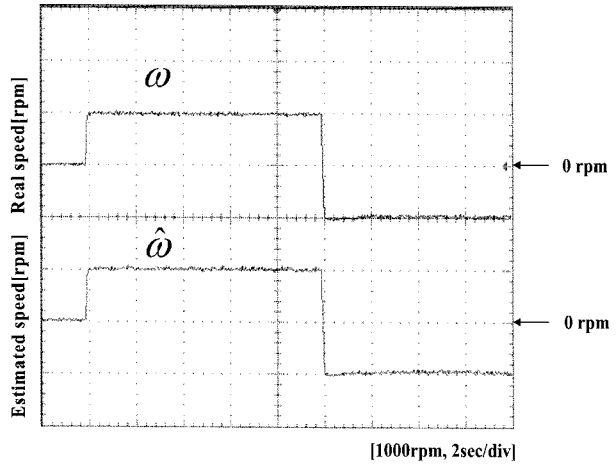

Fig. 7. Real (upper) and estimated speed (lower) when the speed is reversed from 1000[rpm] to -1000[rpm] with no load.

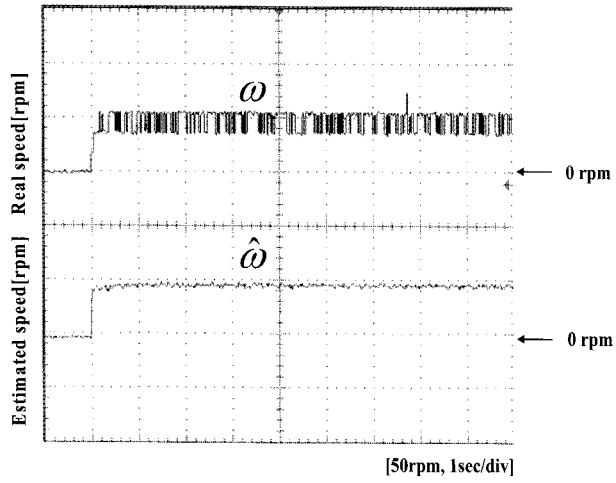

Fig. 8. Real (upper) and estimated speed (lower) when the IPMSM is driven at 50rpm with no load

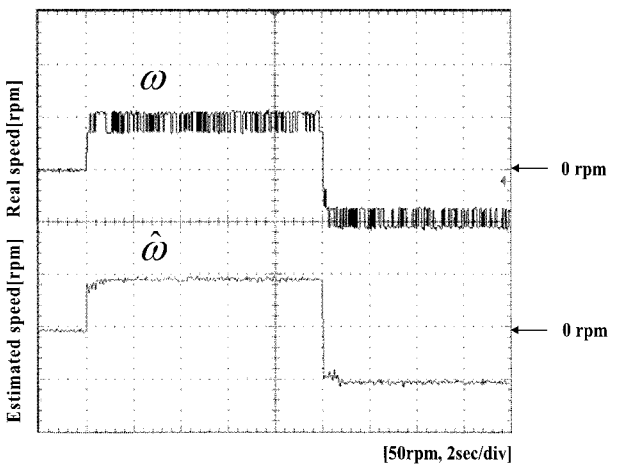

Fig. 9. Real(upper) and estimated speed (lower) when the speed is reversed from 50[rpm] to -50[rpm] with no load.

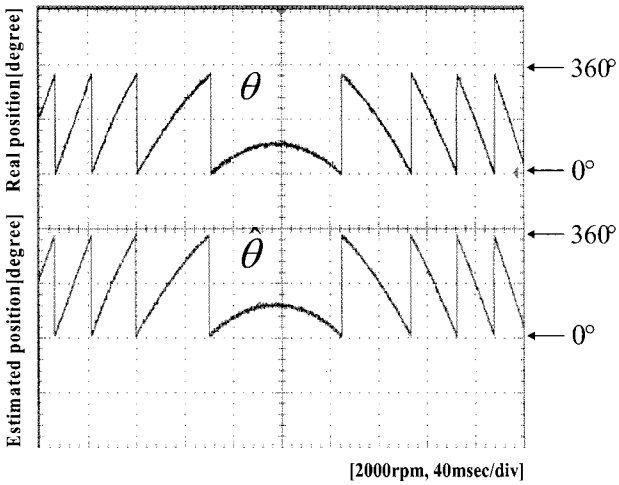

Fig. 10. Real (upper) and estimated position (lower) when the speed is reversed from 2000[rpm] to -2000 [rpm] with no load.

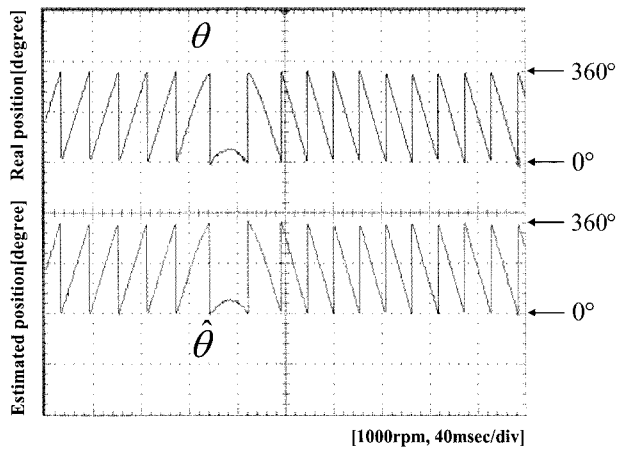

Fig. 11. Real (upper) and estimated position (lower) when the speed is reversed from 1000[rpm] to -1000 [rpm] with no load.

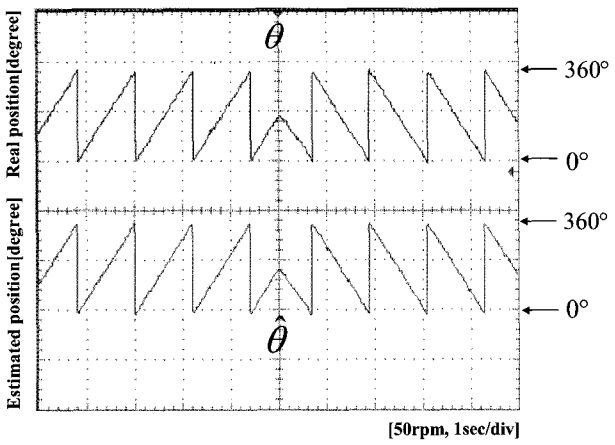

Fig. 12. Real (upper) and estimated position (lower) when the speed is reversed from 50rpm to -50rpm with no load

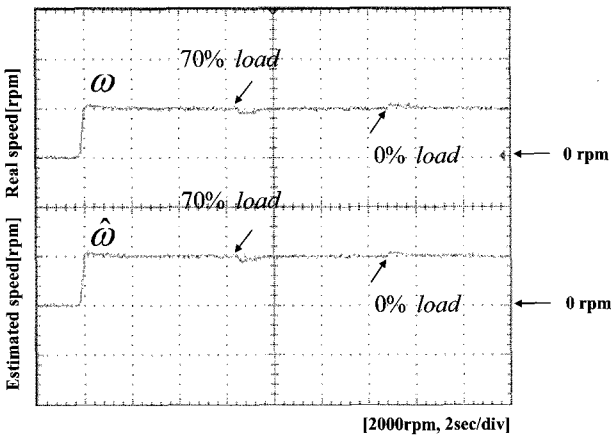

Fig. 13. Real (upper) and estimated speed (lower) at 2000rpm when the load is changed from 0% to 70% and returned to 0%

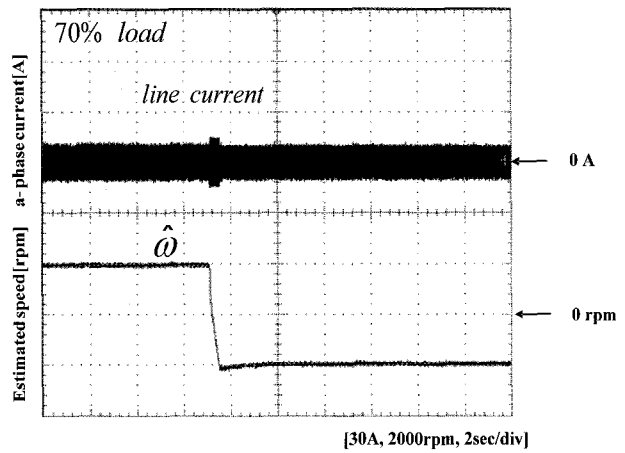

Fig. 14. Line current (upper) and estimated speed (lower) when the speed is reversed from 2000[rpm] to -2000[rpm] with 70% load.

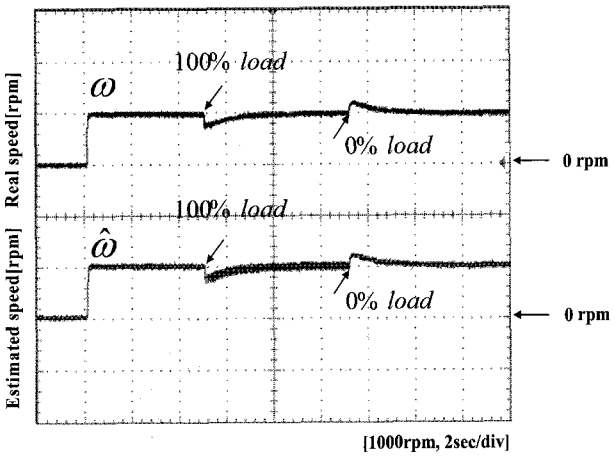

Fig. 15. Real (upper) and estimated speed (lower) at 1000 rpm when the load is changed from 0% to 100% and returned to 0%

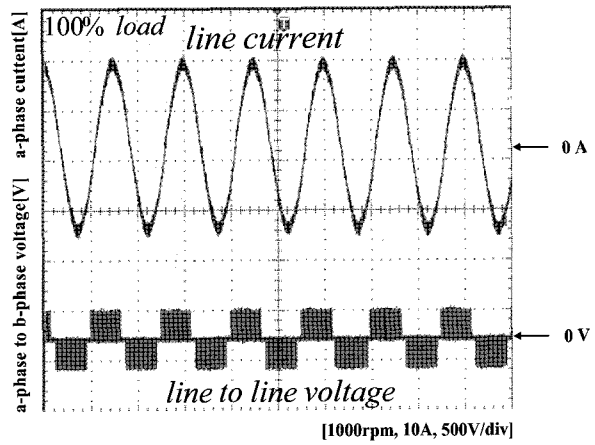

Fig. 16. Line current (upper) and line to line voltage (lower) when the IPMSM is driven at 1000rpm with 100% load

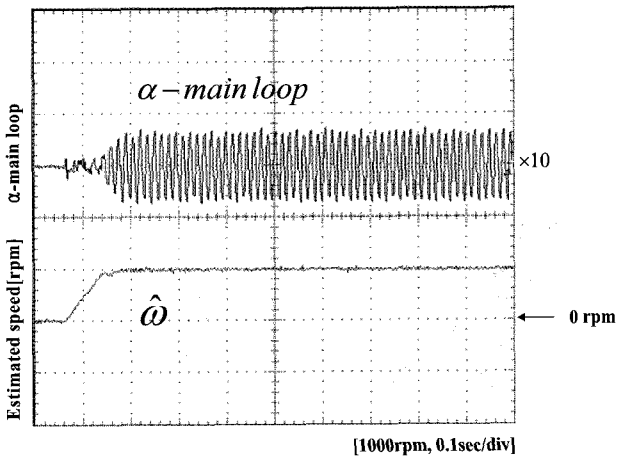

Fig. 17. α -main loop (upper) and estimated speed (lower) when the IPMSM is driven at 1000rpm with no load

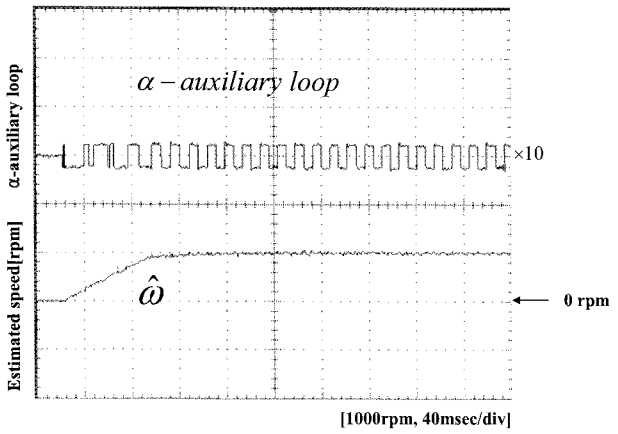

Fig. 18. α-auxiliary loop (upper) and estimated speed (lower) when the IPMSM is driven at 1000rpm with no load

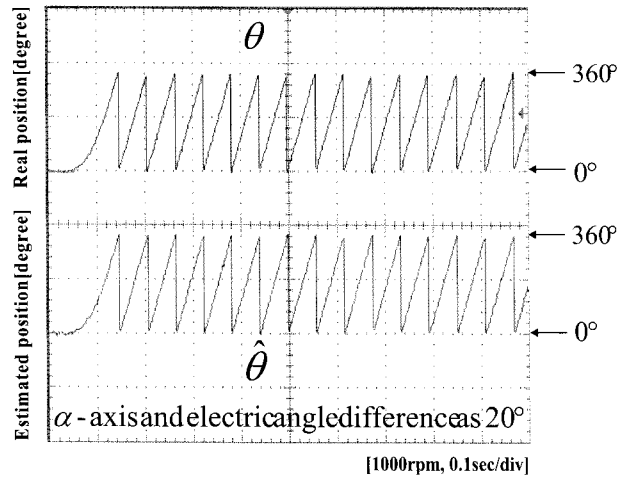

Fig. 19. Real (upper) and estimated (lower) position when the IPMSM is driven at 1000rpm with d-axis and electric angle difference of 20°

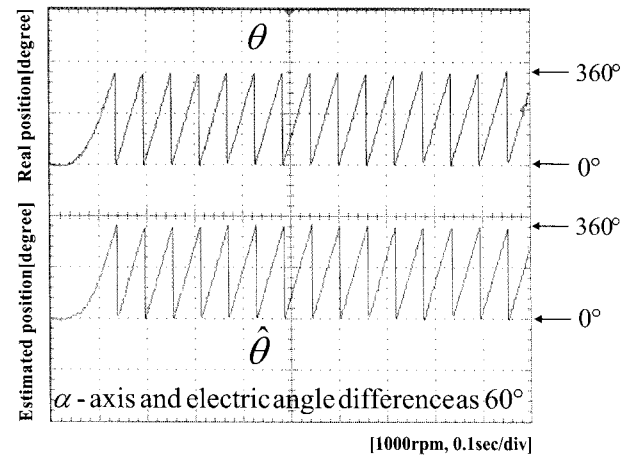

Fig. 20. Real (upper) and estimated (lower) position when the IPMSM is driven at 1000rpm with d-axis and electric angle difference of 60°

4. Conclusion

In this paper, the observer structure and its design method for an IPMSM are developed, and applied to sensorless vector controls of the speed and position for an IPMSM. Experiment results indicate that the proposed observer yields good estimation performance without chattering problems or estimation errors. Also, it is confirmed that the system of the proposed observer estimates the rotor speed and the rotor position well at the steady and transient state. Operation at low and variable speed as well as high speed has robustness in a wide range of operation characteristics as well as in the case of imposed load and starting error. Thus, using only a voltage equation, sensorless vector control of an IMPSM can be realized as it is not sensitive to changes of the parameters induced by the mechanical coefficient.

Acknowledgements

This work was supported by an Inha University Research Grant.

References

[1] Pillay, P., and Krishnan, R., "Modeling, Simulation, and Analysis of Permanent Magnet Motor Drives, part I : The Permanent Magnet Synchronous Motor Drive", IEEE Trans. IA., vol. 25, pp. 265-273, 1989.

[2] Takigawa, Masahiro, et. al., "A Wide Speed Control System for Brushless DC Motor Regarding to the Transient Response Characteristics", IEE. Japan, vol. 113-D, no. 2 pp. 151-158, 1993.

[3] Shouse, K. R., and Taylor, D. G., "Sensorless velocity control of permanent magnet synchronous motors", IEEE Trans. IA., vol. 25, pp. 265-273. 1989.

[4] Hu, J., Zhu, D., Li, Y., Gao, J., "Application of Sliding Observer to Sensorless Permanent Magnet Synchronous Motor Drive System", IEEE PESC Conf. Record, pp. 532-536, 1994.

[5] Sepe, R. B., et. al., "Real-Time Adaptive Control of the Permanent Magnet Synchronous Motor," IEEE Trans. IE., vol. 27, no. 4, pp. 706-714, 1991.

[6] Sepe, R. B., Lang, J. H., "Real-time observer-based (Adaptive) control of a permanent-magnet synchronous motor without mechanical sensor", IEEE Trans. Ind. Appl., vol. 28, no. 6, pp. 1345-1352, 1992.

[7] Kim, Y. C., et al, "A Position Sensorless Control for Brushless DC Motor using Binary Observer", ICPE Conf. Rec, pp. 546-551, 1995.

[8] Slotine, J-J E., Li, W., "Applied Nonlinear Control," from Prentice-Hall, 1991.

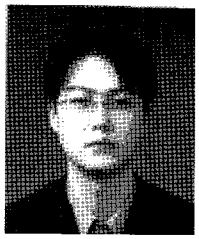

Hyoung-Seok Kang received his B.S. degree in Electronic Engineering, Dongyang University, Korea, in 2003, and his M.S. degree in Electronic Engineering and his Ph.D. degree in Electrical Engineering from Inha University, Korea, in 2005 and 2009, respectively. He is currently working as a Researcher at Samsung Techwin Co., LTD.

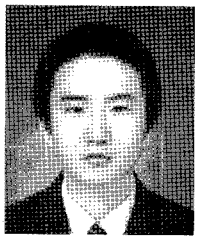

Cheon-Kyu Kim received his B.S. and M.S. degrees in Electrical Engineering from Inha University, Korea, in 2007 and 2009, respectively. He is currently working as a Researcher at LG Electronics Co., LTD.

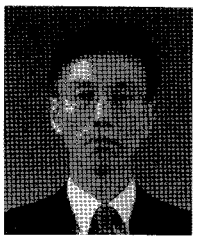

Young-Seok Kim received his B.S. degree in Electrical Engineering from Inha University, Korea, in 1997, and his M.S. and Ph.D. degrees in Electrical Engineering from Nagoya University, Japan, in 1984 and 1987, respectively. In 1989, he joined Inha University in Korea where he is currently a Professor in the Division of Electrical Engineering.